

# Dynamical properties of a few mass-imbalanced ultra-cold fermions confined in a double-well potential

Dillip K. Nandy & Tomasz Sowiński

Institute of Physics, Polish Academy of Sciences, Aleja Lotnikow 32/46, PL-02668  
Warsaw, Poland

E-mail: nandy@ifpan.edu.pl

**Abstract.** A comprehensive analysis of the exact unitary dynamics of two-component mass-imbalanced fermions in a one-dimensional double-well potential is accomplished by considering the total number of particles maximum up to six. The simultaneous effect of mass imbalance between the flavors and their mutual interaction on the particle dynamics is scrutinized through exact diagonalization. In particular, we investigate the occupation dynamics of such a system with two experimentally accessible initial states: spatially separated two-component systems and maximally one atom paired up scenario. Besides, the occupation dynamics we have also examined the evolution of the single-particle von Neumann entanglement entropy to assess the correlation of a fermionic impurity atom within the fermionic bath of the other component.

## 1. Introduction

The monumental progress in the field of laser cooling and trapping of a few microscopic particles obeying any statistics has opened up a new window in the area of quantum engineering [1, 2, 3, 4]. In the contemporary experiments, it is not only possible to efficiently control the number of particles of various flavors confined in an arbitrary trap potential but also their mutual interactions [3, 5, 6]. Such unprecedented control over atom number and their interactions have provided a route to address many theoretical questions about the physical properties of these mesoscopic systems which so far not been completely understood [7, 8]. Among the unanswered questions, the transition from two-body to the many-body system can be well characterized by employing various many-body techniques of condensed matter physics. For example in the recent past, Wenz *et al.* for the first time have investigated such crossover from few- to the many-body regime in a quasi-one-dimensional system of ultracold atoms. In this, they studied the emergence of Fermi sea by increasing the number of identical fermions one-by-one which are interacting with a single impurity atom in it [9]. Further, the concept of two-body pairing in the case of attractive interactions of ultra-cold atoms as a function of system size was also observed in the experiment [10] and theoretically addressed in many studies [10, 11, 12].

Recently, simultaneous trapping of two-component fermions of different mass has gained considerable interest to both experimentalists and theorists [13, 14, 15, 16]. In this kind of system, the additional parameter that is the mass ratio between the flavors offers an extra degree of freedom which makes the system behave differently than the usual equal mass counterpart [17, 18, 19, 20, 21, 22, 23, 24, 25, 26]. One of the interesting signatures of these mass imbalanced fermionic systems is that for sufficiently large mass ratios they can exhibit a specific separation between lighter and heavier components depending on the shape of an external trap [27, 28, 29, 30]. Furthermore, it has been investigated using many sophisticated many-body techniques that the ground-state phase diagrams of this mass- and population-imbalanced two-component Fermi systems show some topological properties in contrast to the equal mass fermionic systems [21, 22, 23, 26]. Owing to this mass difference of these two-component mixtures the trapping potential felt by each flavor is in general different. Experimentally one has the flexibility to change the shape of the trapping potential to some degree [24, 31]. From this point of view, these systems also show some similarity to population imbalanced systems of equal mass flavors [32, 33]. Currently, many experiments in progress focus on these two-component mass-imbalanced fermions [5, 6, 13, 14].

Motivated by these intriguing experiments, here, we investigate the dynamical behavior of the two-component mass-imbalanced few-fermion system confined in a one-dimensional double-well trapping potential. Double-well confinement gives the simplest example where the truly quantum dynamical behavior of the systems can be explored. For instance, the physics of the celebrated Josephson effect [34], p-n junctions [35, 36], and many other atomtronic devices can be accomplished by the knowledge of single-particle tunneling through the classically forbidden region of the double-well barrier. Further, these simplest systems could be more realistic and interesting by taking into account the mutual interaction between the particles. In many recent experiments with ultra-cold atoms forming Bose-Einstein condensate, double-well systems are commonly exploited [37, 38, 39, 40, 41, 42, 43]. However, ultra-cold fermionic mixtures confined in a double-wells are also accessible [44].

The dynamical behavior of the two-component fermionic and bosonic systems corresponding to the equal mass case in a different kind of double-well potential with a few particles was recently investigated [11, 45]. Here, we focus on the mass-imbalanced case to study the dynamics of initially prepared fermionic flavors and try to answer the questions on the role of mutual interaction. Starting with a minimal system with two particles, we analyze the many-body effect on the system dynamics by increasing the total number of particles maximum up to six. For the experimental relevance, we consider the case with a mass ratio,  $40/6$ , which corresponds to the mass of  $^{40}\text{K}$  and  $^6\text{Li}$ . Owing to such practical relevance we show the time dynamics explicitly for this mass ratio in all the system sizes we study here.

## 2. The Model

In the present study, we consider a two-flavor system of a few ultra-cold fermions interacting via a short-range delta-like potential and confined in a one-dimensional external trap having double-well shape. Such a system is described by the Hamiltonian of the form

$$\hat{\mathcal{H}} = \sum_{\sigma} \int dx \hat{\Psi}_{\sigma}^{\dagger}(x) H_{\sigma} \hat{\Psi}_{\sigma}(x) + g \int dx \hat{\Psi}_{\uparrow}^{\dagger}(x) \hat{\Psi}_{\downarrow}^{\dagger}(x) \hat{\Psi}_{\downarrow}(x) \hat{\Psi}_{\uparrow}(x), \quad (1)$$

where  $\hat{\Psi}_{\sigma}(x)$  is the fermionic field operator annihilating particle of spin  $\sigma$  at position  $x$ ,  $g$  is an effective interaction coupling and  $H_{\sigma}$  is a single-particle Hamiltonian describing motion of  $\sigma$ -component particle. In general, the single-particle Hamiltonians may significantly depend on the component since different species experience external electromagnetic fields differently. Here, we assume that they have a form [46, 15, 16]

$$H_{\sigma} = -\frac{\hbar^2}{2m_{\sigma}} \frac{d^2}{dx^2} + \frac{m_{\sigma}\Omega^2}{2} x^2 + \frac{\lambda}{\sqrt{\pi}\sigma} e^{-x^2/\sigma^2}. \quad (2)$$

This assumption simply means that both species are confined in a one-dimensional harmonic trap of the same frequency  $\Omega$  which is additionally split to two wells by central well of width  $\sigma$  and strength  $\lambda$ . In this approximation, parameters  $\lambda$  and  $\sigma$  are independent on the component. This simplification is experimentally justified since the parameters are controlled mostly by the intensity and the width of the additional laser beam. If one expresses all quantities in the natural units of the harmonic oscillator related to one of the flavors (in the following we choose the spin-down component) then the single-particle Hamiltonians have a form

$$H_{\downarrow} = -\frac{1}{2} \frac{d^2}{dx^2} + \frac{1}{2} x^2 + \frac{\lambda}{\sqrt{\pi}\sigma} e^{-x^2/\sigma^2}, \quad (3a)$$

$$H_{\uparrow} = -\frac{1}{2\mu} \frac{d^2}{dx^2} + \frac{\mu}{2} x^2 + \frac{\lambda}{\sqrt{\pi}\sigma} e^{-x^2/\sigma^2}, \quad (3b)$$

where  $\mu = m_{\uparrow}/m_{\downarrow}$  is a mass ratio between different components' atoms. In figure 1(a) and figure 1(b) we present a shape of potential for different parameters and in figure 1(c) the single-particle spectra for fixed  $\sigma$  as a function of the barrier height  $\lambda$ . Black and red lines correspond to spectra of light ( $m_{\downarrow} = 1$ ) and heavy ( $m_{\uparrow} = 40/6$ ) component, respectively. As suspected, for vanishing barrier ( $\lambda = 0$ ) harmonic spectrum for both components is reproduced, while in the limit of very deep wells ( $\lambda \rightarrow \infty$ ) two-fold degeneracy between successive even and odd states is obtained.

For dynamical problems in a double-well potential it is convenient to introduce a basis of states localized in the left ( $\psi_{Li}$ ) and in the right ( $\psi_{Ri}$ ) well of the potential. They can be formed by simply taking the linear combinations of neighboring eigenstates  $\phi_i^{\sigma}$  of the single-particle Hamiltonians (3a) of the respective flavors:

$$\psi_{Li}^{\sigma} = \frac{1}{\sqrt{2}}(\phi_{2i}^{\sigma} - \phi_{2i-1}^{\sigma}), \quad (4a)$$

$$\psi_{Ri}^{\sigma} = \frac{1}{\sqrt{2}}(\phi_{2i}^{\sigma} + \phi_{2i-1}^{\sigma}). \quad (4b)$$

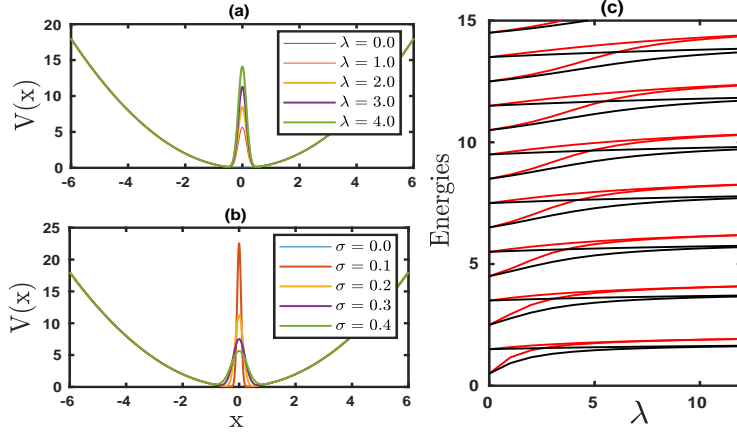


**Figure 1.** Shapes of considered external potential for (a) different barrier heights  $\lambda$  and fixed  $\sigma = 0.2$  (b) different  $\sigma$  values at the barrier height  $\lambda = 4.0$  (c) Low-lying energy spectra for the single-particle Hamiltonians (3a) as a function of  $\lambda$  with  $\sigma = 0.2$  for  $\mu = 40/6$ . The energy levels shown as red and black lines correspond to light and heavy particles, respectively.

One can check that these redefined sets of orbitals also obey the orthonormality condition, however, they are no longer eigenstates of the single-particle Hamiltonian. Using these localized single-particle basis, the fermionic field operators can be expressed as

$$\hat{\Psi}_{\uparrow}(x) = \sum_i \left[ \psi_{Li}^{\uparrow}(x) \hat{a}_{Li} + \psi_{Ri}^{\uparrow}(x) \hat{a}_{Ri} \right] \quad (5a)$$

$$\hat{\Psi}_{\downarrow}(x) = \sum_i \left[ \psi_{Li}^{\downarrow}(x) \hat{b}_{Li} + \psi_{Ri}^{\downarrow}(x) \hat{b}_{Ri} \right], \quad (5b)$$

where  $\hat{a}$  and  $\hat{b}$  are the annihilation operators for the  $\uparrow$ - and  $\downarrow$ - types of fermions, respectively. With the above decomposition of field operators one can now write the Hamiltonian (1) as

$$\begin{aligned} \hat{\mathcal{H}} = & \sum_i E_{i\uparrow} \left[ \hat{a}_{Li}^{\dagger} \hat{a}_{Li} + \hat{a}_{Ri}^{\dagger} \hat{a}_{Ri} \right] + \sum_i E_{i\downarrow} \left[ \hat{b}_{Li}^{\dagger} \hat{b}_{Li} + \hat{b}_{Ri}^{\dagger} \hat{b}_{Ri} \right] \\ & + \sum_i t_{i\uparrow} \left[ \hat{a}_{Li}^{\dagger} \hat{a}_{Ri} + \hat{a}_{Ri}^{\dagger} \hat{a}_{Li} \right] + \sum_i t_{i\downarrow} \left[ \hat{b}_{Li}^{\dagger} \hat{b}_{Ri} + \hat{b}_{Ri}^{\dagger} \hat{b}_{Li} \right] \\ & + g \sum_{ijkl} \sum_{\vec{\alpha}} U_{ijkl}^{\vec{\alpha}} \hat{a}_{\alpha_1 i}^{\dagger} \hat{b}_{\alpha_2 j}^{\dagger} \hat{b}_{\alpha_3 k} \hat{a}_{\alpha_4 l} \end{aligned} \quad (6)$$

where  $E_{i,\sigma}$  and  $t_{i,\sigma}$  can be found as [11]

$$\begin{aligned} E_{i,\sigma} &= (\varepsilon_{2i+1,\sigma} + \varepsilon_{2i,\sigma})/2, \\ t_{i,\sigma} &= (\varepsilon_{2i+1,\sigma} - \varepsilon_{2i,\sigma})/2. \end{aligned} \quad (7)$$

Here,  $\vec{\alpha} = (\alpha_1, \alpha_2, \alpha_3, \alpha_4)$  is an algebraic vector of “left- right” indices holding the fact that all four operators come with their own left or right basis state. Interaction

energies can be calculated directly from the shape of localized functions

$$U_{ijkl}^{\vec{\alpha}} = \int dx \psi_{\alpha_1 i}^*(x) \psi_{\alpha_2 j}^*(x) \psi_{\alpha_3 k}(x) \psi_{\alpha_4 l}(x) \quad (8)$$

### 3. The Method

The dynamical behavior of the system is studied by solving the time-dependent many-body Schrödinger equation. In our numerical approach, we first construct the matrix form of the many-body Hamiltonian (6) in the Fock basis by using the redefined single-particle orbitals (2). In the next step, for a given interaction  $g$ , we do the exact diagonalization of this constructed Hamiltonian to obtain many-body eigenstates  $|E_n\rangle$  with corresponding eigenenergies  $E_n$ . As the Hilbert space size grows exponentially with the number of orbitals, we truncate the single-particle orbitals by a reasonable cutoff value which of course depends on the system's size and also on the interaction. Nevertheless, for the interaction range, we are interested here, we find that for most of the system size the results are hardly affected by the inclusion of higher orbitals than the cutoff values.

Here, we assume that the evolution is unitary and governed solely by the many-body Hamiltonian (1). Therefore, having the system initially prepared in the state  $|\text{ini}\rangle$  the state of the system evolves as

$$|\Phi(t)\rangle = \sum_n e^{-iE_n t} C_n |E_n\rangle, \quad (9)$$

where the coefficients  $C_n = \langle E_n | \text{ini} \rangle$ . In principle, the summation index can run over full Hilbert space dimension, however it is always crucial, especially for large Hilbert space dimension, to find a suitable number of eigenstates that can yield the desired results. In practice, this can be achieved by determining the initial fidelity  $F = |\langle \Phi(0) | \text{ini} \rangle|^2$ . Here, we ensure that the fidelity is always larger than 99% in all the cases. Having the state of the system at any moment  $|\Phi(t)\rangle$  we can determine different observables which are accessible experimentally. The simplest are related to the single-particle density profiles of the form

$$\rho_\sigma(x) = \langle \Phi(t) | \hat{\Psi}_\sigma^\dagger(x) \hat{\Psi}_\sigma(x) | \Phi(t) \rangle. \quad (10)$$

Although the profiles are well understood quantities, the macroscopic flow between the wells is described much better in the language of integrated quantities. Therefore, for further convenience we introduce the occupation numbers in the left and right well as

$$N_{L\sigma} = \int_{-\infty}^0 dx \rho_\sigma(x), \quad N_{R\sigma} = \int_0^{\infty} dx \rho_\sigma(x). \quad (11)$$

### 4. Two-particle system

We start the discussion of the dynamics with the simplest case of two opposite-spin fermions. Before going to the detailed analysis of the dynamics, we first draw

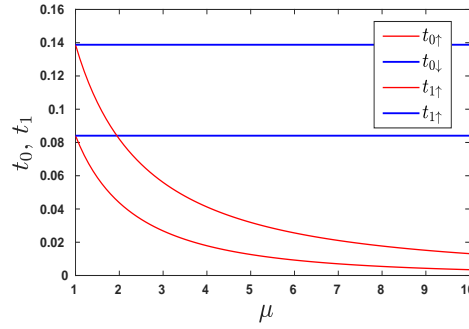


**Figure 2.** Behavior of the leading-order single-particle tunneling amplitudes  $t_{0,\sigma}$  and  $t_{1,\sigma}$  as functions of mass ratios using  $\lambda = 4.0$  and  $\sigma = 0.2$ .

attention to the behavior of the leading order single-particle tunneling amplitudes as a function of the mass ratios of both types of flavors. As an example in figure 2 we show the single-particle tunneling amplitudes  $t_{0,\sigma}$  and  $t_{1,\sigma}$  as function of the mass ratio  $\mu$ . From this plot, it is clear that as the mass ratio is increased the tunneling amplitudes are suppressed monotonically. Since our single-particle Hamiltonians are expressed in units of the lighter flavor, therefore only changes in the heavier flavor amplitudes are noticed in this plot. From now, unless stated otherwise, the dynamical properties are displayed explicitly for the  $\mu = 40/6$  case corresponding to  ${}^6\text{Li}$ - ${}^{40}\text{K}$  mixture. Note, that each double-well confinement there exists a specific mass ratio for which the tunneling amplitude of a heavier particle in the first excited band  $t_{1\uparrow}$  is equal to the tunneling amplitude of a lighter particle in a ground band  $t_{0\downarrow}$ .

In the case of two particles we consider two different initial states. First, we assume that particles initially occupy opposite wells in the ground band, *i.e.*, the initial state has a simple form  $|\text{ini}_1\rangle = a_{L0}^\dagger b_{R0}^\dagger |\text{vac}\rangle$ . In the second case we relax the condition of minimum energy configuration and we consider the scenario when the heavier particle is singly excited in its well,  $|\text{ini}_2\rangle = a_{L1}^\dagger b_{R0}^\dagger |\text{vac}\rangle$ . In this way we are able to examine behavior of the system when we cross the resonance condition for tunneling amplitudes mentioned above. Pictorially, both initial configurations are shown in the left panel of figure 3.

It is instructive to start the analysis by plotting the many-body spectrum as a function of interaction  $g$  and compare it with the average energy in the initial states. Since in both initial states considered particles are spatially separated, the interaction energy  $\langle \text{ini} | \hat{\mathcal{H}} | \text{ini} \rangle$  is almost negligible and it almost does not depend on  $g$ . In contrast, the many-body spectrum is interaction sensitive. By direct comparison of these energies (see figure 4(a)) one can notice that for some particular interaction strengths on the negative branch, possible energy matching occurs. Since evolution is an energy-conserving process, we may suspect that for these specific interactions some changes of the dynamical properties may be present.

To get a better view on dynamical properties of the system we focus on time

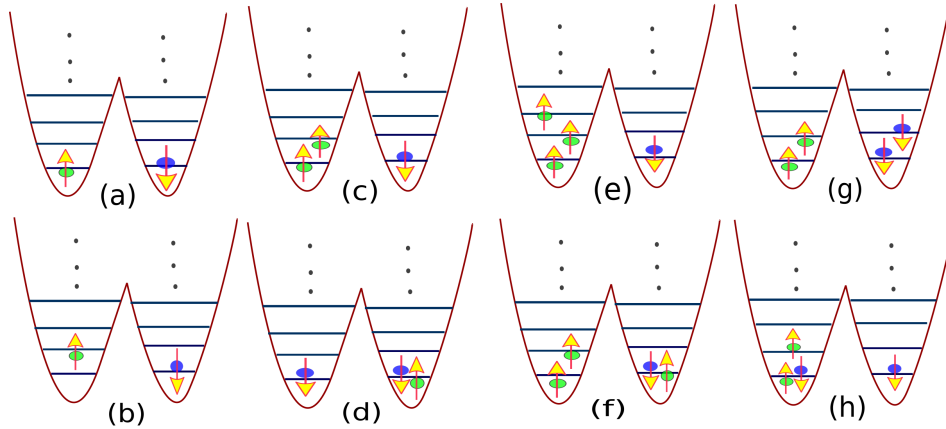


**Figure 3.** (color online) Pictorial representation of different initial configurations of  $N = 2, 3$ , and 4 particles systems considered in the main text. The green balls with up arrow and the blue ball with down arrow in general represent two kind of fermionic components. Horizontal lines drawn in each well refer to the orbitals of the single-particle Hamiltonian.

evolution of occupations (11) (see figure 4(b) for initial state  $|ini_1\rangle$ ). Since in the initial state  $|ini_1\rangle$  both particles occupy the lowest band, in the case of non-interacting system the dynamics is governed solely by  $t_{0\uparrow}$  and  $t_{0\downarrow}$  tunneling amplitudes. When interactions increase towards repulsions or attractions we observe significant suppression of the tunneling. This fact is a direct manifestation of energy conservation – single-particle tunnelings lead to states having both particles occupying the same well. Many-body energies of these states however, due to the interaction energy, do not match the initial energy of the system. Only in the second-order process the state with the same energy having particles interchanged may be reached. This process however has the effective amplitude suppressed by interactions,  $t_{0\uparrow}t_{0\downarrow}/|g|$ . For repulsive interactions, this phenomenological argumentation is always valid since interactions cannot connect the initial state to any other many-body state having substantially different many-body energy. The situation is a little bit different for attractive forces. As noticed above, for some particular interaction strengths, highly excited many-body states may have exactly the same energy as the energy of the initial state. Since coupling to these states is provided by interaction terms, energy-conservative evolution may be much richer. Our numerical calculations fully support this observation. As it is seen in figure 4 for  $g \approx -2.4$ ,  $g \approx -3.6$ , etc. the tunneling is enhanced and particles freely exchange their wells. The complete dynamical picture as a function of interactions is given in figures 4(c)-(d) and clearly indicates different tunneling regimes for both the species.

Additionally, to make the analysis more comprehensive, we artificially also examined the model with single-particle tunneling terms completely switched off. It turns out that, although the single-particle terms play a dominant role far from these resonant points, their importance is negligible at resonances where a whole dynamics

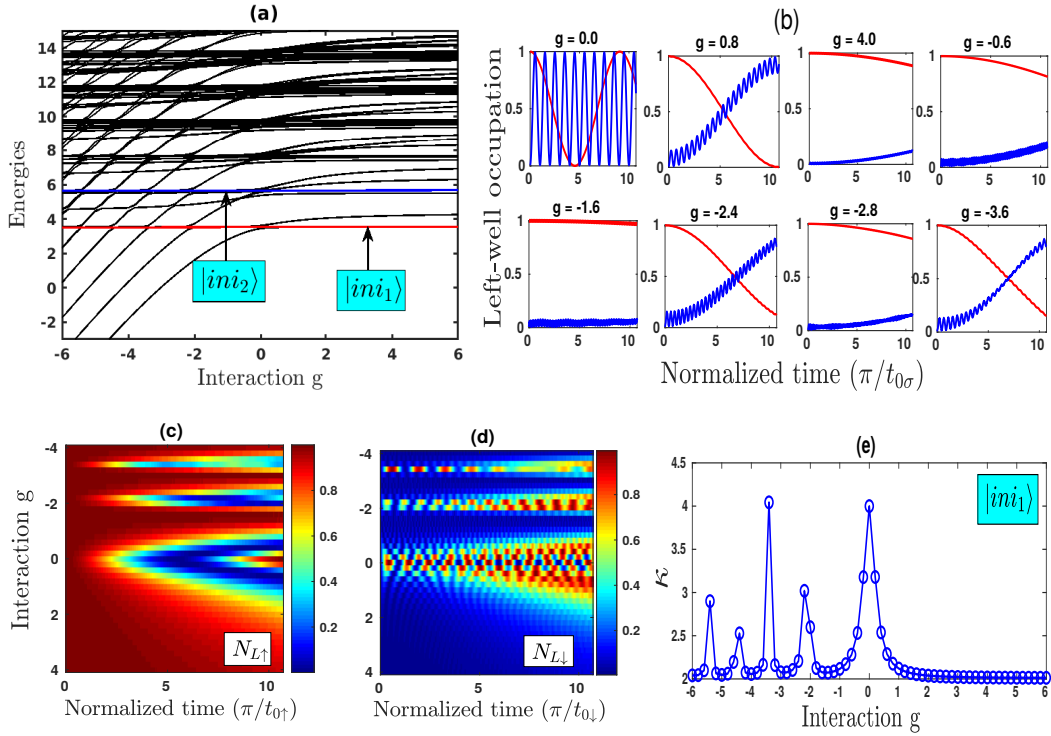


**Figure 4.** Energy spectrum of the many-body Hamiltonian (equation (1)) for  $N_{\uparrow} = N_{\downarrow} = 1$  particles with  $\mu = 40/6$  as a function of interaction strength  $g$ . The thick red and blue lines correspond to the energy of initial states  $|ini_1\rangle$  and  $|ini_2\rangle$ , respectively. Double-well potential parameters set as  $\sigma = 0.2$  and  $\lambda = 4.0$ . (b) Occupations of the left well as a function of time for different interactions for a system prepared in the initial state  $|ini_1\rangle$ . Typically, interactions suppressed tunnelings but for particular interactions the dynamics through the barrier is enhanced. See the main text for explanation. (c-d) Complete dynamics of the left-well occupation number of the heavier (b) and lighter (c) component for the whole range of interaction parameter. (e) Effective number of many-body eigenstates contributing to the initial state  $|ini_1\rangle$  as a function of interactions. Note, significant increase of this parameter at resonant interaction strengths.

is governed solely by interaction terms. Finally, let us note, that a very similar mechanism is present for the second initial state  $|ini_2\rangle$ . Although single-particle tunneling for the excited particle is different, interactions play exactly the same role – they suppress density flow when couplings to other many-body states violate conservation of the energy and they enhance collective tunneling whenever other many-body states are accessible without this violation. Importantly and surprisingly, our numerical calculations show that no significant change of this behavior is present when the resonant condition  $t_{0\uparrow} = t_{1\downarrow}$  between tunneling is reached for the initial state  $|ini_2\rangle$ .

The suppression or enhancement of the density flow through the barrier can be also explained by inspecting the decomposition of the initial state to the many-



body eigenstates of the Hamiltonian. In fact, the dynamics of the system is governed only by a few eigenstates dominating in the initial state. To quantify this number of eigenstates, we analyze the properties of the decomposition coefficients  $C_n$  defined in (9) by calculating the quantity

$$\kappa = \frac{1}{\sum_n |C_n|^4}. \quad (12)$$

The quantity  $\kappa$  (known also as Schmidt decomposition in the Random matrix theory) essentially determines an effective number of many-body eigenstates taking part in the decomposition of an initial state. As shown in the figure 4(d), whenever interaction strength  $g$  is close to the resonant value the number  $\kappa$  significantly increases. It simply means that a larger number of states take part in determining the dynamics of the system and substantially change its properties.

At this point it should be mentioned that even in the cases when density flow between wells is strongly suppressed by interactions the many-body state of the system continuously evolves. It can be clearly visible when correlations between particles are considered. To show it, let us focus on the single-particle von Neumann entropy defined as

$$S_\sigma(t) = - \sum_k \lambda_k^\sigma(t) \ln \lambda_k^\sigma(t), \quad (13)$$

where  $\lambda_k$  denotes the eigenvalues of the single-particle reduced density matrix of the form

$$\rho(x, x') = \langle \Phi(t) | \hat{\Psi}_\sigma^\dagger(x) \hat{\Psi}_\sigma(x') | \Phi(t) \rangle. \quad (14)$$

Correspondingly to figure 4, in figure 5 we display time evolution of the entropy for different interactions. Initially, particles occupying opposite wells are uncorrelated and the entropy vanishes. However, even in the cases when density flow is frozen and particles remain in their initial wells, correlations between particles are build-up and entropy significantly increases.

To give a better understanding of the dynamics let us look closer to the Fock-space decomposition of the many-body eigenstates contributing to the initial state. In particular, it is interesting to find this decomposition for interactions for which the density flow is significantly restrained. As we obtained from the decomposition, the effective number of eigenstates contributing to the dynamics is around  $\kappa \approx 2$ , *i.e.*, only two eigenstates provide a whole dynamics of the system. It is a matter of fact, that the Fock-space decomposition of these two eigenstates (say  $|E_1\rangle$  and  $|E_2\rangle$ ) is very simple – they can be almost perfectly expressed as a linear combination of the initial state  $|ini\rangle$  and its respective mirror reflection. For example, if initially the system is prepared in the state  $|ini_1\rangle = a_{L0}^\dagger b_{R0}^\dagger |\text{vac}\rangle$  then the second Fock state present in the decomposition is  $|ini'_1\rangle = a_{R0}^\dagger b_{L0}^\dagger |\text{vac}\rangle$ . Hence, as a consequence of very strong interactions, a description of the whole system is significantly simplified and the dynamics of the many-body system can be viewed as a simple two-level system. We

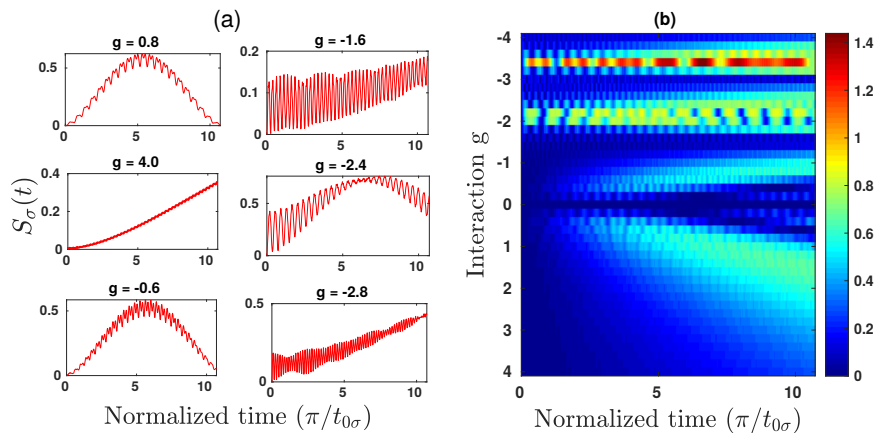


**Figure 5.** (Color online) (a) Evolution of the single-particle von Neumann entropy at different interaction values:  $g = 0.8, 4.0, -0.6, -1.6, -2.4$  and  $-2.8$  corresponding to plots in Fig. 4a. (b) Dynamics of entropy for the complete range of interaction parameter considered in our calculations. One can see a finite correlations between the system for very large value of repulsions and attractions away from the resonances points for which the occupation dynamics is highly decreased (as shown in the figure4).

checked that this mechanism is generic for any initial state provided that interactions strongly suppress the density flow.

## 5. Three-particle system

In this section we investigate dynamical properties of the system with one more particle added to the heavier or lighter component of the two-particle system. This is the minimal system for which the quantum statistics between indistinguishable particles has to be taken into account. Similarly as in the case of  $N = 2$ , here also we intend to study the dynamics when the two flavors are initially prepared in the distinct wells. Depending on situations, we distinguish two initial states:  $|\text{ini}_3\rangle = a_{L0}^\dagger a_{L1}^\dagger b_{R0}^\dagger |\text{vac}\rangle$  and  $|\text{ini}_4\rangle = a_{R0}^\dagger b_{L0}^\dagger b_{L1}^\dagger |\text{vac}\rangle$ , for  $N_\uparrow = 2, N_\downarrow = 1$  and  $N_\uparrow = 1, N_\downarrow = 2$  cases respectively (see figure 3(c) for schematic representation). Moreover, to make the discussion as comprehensive as possible, we additionally consider two other initial states which can be also well-prepared experimentally:  $|\text{ini}_5\rangle = a_{L0}^\dagger a_{R0}^\dagger b_{R0}^\dagger |\text{vac}\rangle$  and  $|\text{ini}_6\rangle = a_{R0}^\dagger b_{L0}^\dagger b_{R0}^\dagger |\text{vac}\rangle$ , for  $N_\uparrow = 2, N_\downarrow = 1$  and  $N_\uparrow = 1, N_\downarrow = 2$  cases respectively. In these initial configurations (see figure 3(d) for schematic representation) two particles of opposite spins are paired in a chosen well and the remaining third particle occupies the opposite well.

The energy spectra for both situations ( $N_\uparrow = 2, N_\downarrow = 1$  and  $N_\uparrow = 1, N_\downarrow = 2$ ) are shown in figure 6(a) and figure 6(b), respectively along with average energies of their corresponding initial states. Exactly, as in the case of two-particle system we find the energy of the initial states  $|\text{ini}_3\rangle$  and  $|\text{ini}_4\rangle$  (shown as thick red lines)

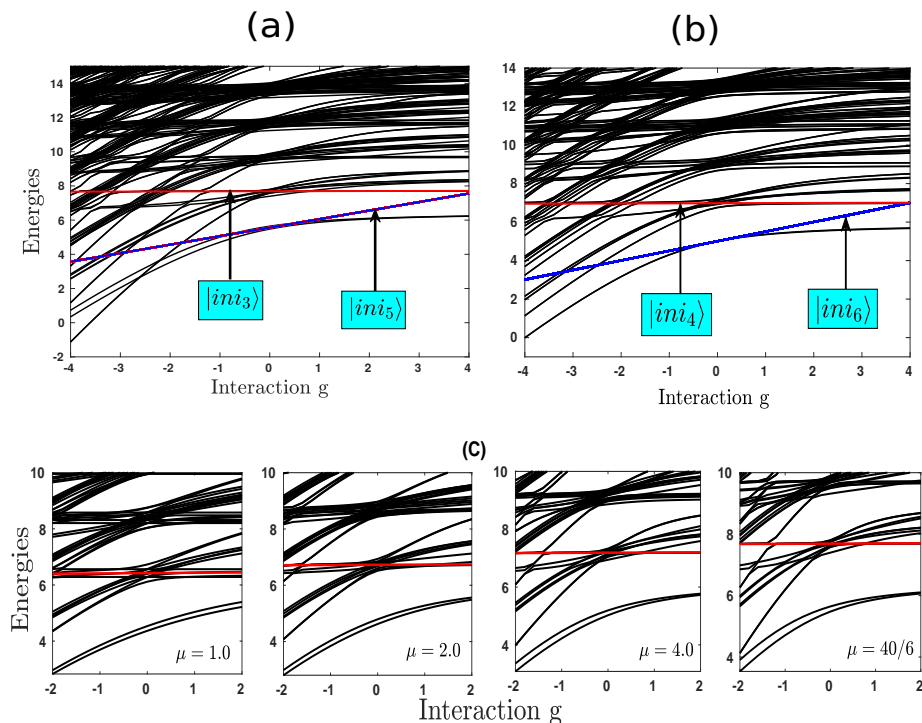


**Figure 6.** (Color online) (a) and (b) First 500 energy levels of the many-body Hamiltonian as a function of interaction strength  $g$  with  $\mu = 40/6$  for the system  $N_{\uparrow} = 2, N_{\downarrow} = 1$  and  $N_{\uparrow} = 1, N_{\downarrow} = 2$  respectively. The thick red and blue lines refer to energies of various initial state as indicated in the color box. (c) Energies of the  $N_{\uparrow} = 2, N_{\downarrow} = 1$  system calculated with different value of mass ratios between the flavors. It shows effect of mass imbalance on the many-body spectra with respect to the initial state energies as a function of interaction. One can see as the mass ratio is increased a gap is opening between the initial state energies and the system's energies which leads to the suppressed tunneling in the dynamics.

being insensitive to the interaction although they are shifted up in the spectra. On the other hand for the paired initial states  $|ini_5\rangle$  and  $|ini_6\rangle$  (shown as thick blue lines) the energies are no longer insensitive to the interaction. Such behavior is a direct consequence of interactions between the opposite-flavor particles occupying the same well in the initial configuration.

First, let us discuss dynamics of the unpaired state  $|ini_3\rangle$ . The dynamics for the full range of inter-species interaction is shown in figure 7(a)-(b) for the heavier and lighter components respectively. By observing the complete dynamics of this state one can notice for the interacting system the tunneling is effective only for a smaller range of interaction such as  $-0.4 < g < 0.4$ . Moreover, the dynamics show almost a symmetrical behavior in this range and the effect of single-particle hopping is partially compensated by the interaction terms resulting slower dynamics than the non-interacting case. For better understanding we also present the dynamics at some selected interaction points in figure 7(c). Indeed, with such small value of interactions ( $g \sim |0.2|$ ) the two components can tunnel completely to their respective opposite

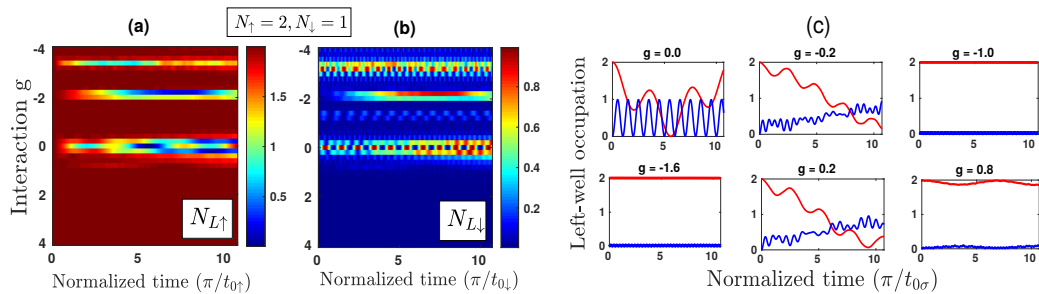


**Figure 7.** (Color online) Left-well occupation dynamics of  $N_{L\uparrow}(t)$  (a) and  $N_{L\downarrow}(t)$  (b) covering the full range of interaction parameter in the three particles systems in the unpaired unpaired form. The evolution is shown for the initial state  $|ini_3\rangle$ . (c) Dynamics of same quantity at some selected interaction points. The blue and red lines refer to the lighter and heavier flavors respectively.

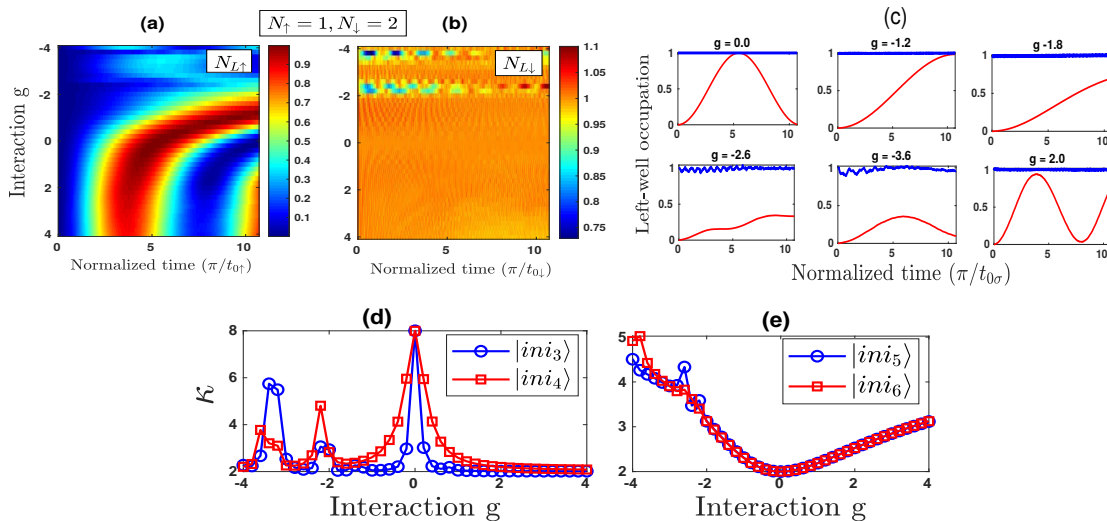


**Figure 8.** (Color online)  $N_{L\uparrow}(t)$  (a) and  $N_{L\downarrow}(t)$  (b) as a function of  $g$ , for the paired initial state  $|ini_6\rangle$  in  $N_{\uparrow} = 1, N_{\downarrow} = 2$  system. (c) dynamics at selected points:  $g = 0.0, -1.2, -1.8, -2.6, -3.6$  and  $g = 2.0$ . (d)-(e) Comparison of eigenstates decomposition of the unpaired and paired initial states in three-particle system.

well with a period of  $t \sim 10(\pi/t_{0\uparrow})$  as is evident from figure 7(c). Then, for the larger value of the repulsions (for example  $g = 0.8$ ), the tunneling is highly suppressed and eventually vanishes. This is due to the complete counter effect between the single-particle tunneling terms and the mutual interaction between the flavors. At this point, we want to emphasize that dynamical properties of the other initial state  $|ini_4\rangle$  is qualitatively very similar and any significant differences are not present.

The complete dynamical situation for the paired state  $|ini_6\rangle$  is shown in the figures 8(a)-(b) and at some specific interactions in figure 8(c). In the zero interaction limit, the Pauli exclusion principle prohibits single-particle tunneling for the lighter flavor in the lowest orbitals. So the dynamics is present only for the particle from the

opposite component. In other words, with the range of mutual interaction considered here, it is not viable to excite the lighter particle into higher orbitals and induce significant tunneling. As can be seen, the heavier atom in the non-interacting limit tunnel completely to the opposite wall with a period  $t \sim 10(\pi/t_{0\uparrow})$ . Afterward, with the increase in attraction, the dynamics become slower and the tunneling amplitude reduces significantly. On the other hand, at the repulsive end, the dynamics is faster than the other counterpart and the tunneling probability becomes almost stationary (see figure 8(c)). Likewise, we analyze the dynamics of the initial state  $|ini_5\rangle$  that show rapid oscillation for the lighter atom in the attractive regime whereas, with the increase in repulsion, the interaction and single-particle terms show a counter effect on the system's dynamics leading to a subsequent decrease in tunneling.

The strong suppression in the tunneling for the unpaired initial states  $|ini_3\rangle$  and  $|ini_4\rangle$  can also be well understood by looking at the response of the energy spectra to the mass-imbalance between the flavors. This is illustrated in the figure 6(c) for different mass ratios:  $\mu = 1.0, 2.0, 4.0$  and  $40/6$ . As can be noticed, specifically at the attractive part, for equal mass case the initial state energy is embedded in the energy levels of the systems as a result of which the system favors a more resonant situation. Thereafter, with the increase in mass ratios, the energy levels are more repelled from the initial state energy and the initial state coincides with one of the eigenstates of the many-body Hamiltonian. Such localization of initial state simply implies the reason for the suppressed dynamics in the range  $-1.9 < g < -0.6$  and for repulsion  $g > 0.6$ . Analogously, one can apply this analysis to the,  $N_\uparrow = 1, N_\downarrow = 2$  system, to explain the effect of mass imbalance on the dynamics.

Let us also mention the Fock-space decomposition of the dominant eigenstates contributing to the dynamics. Exactly as in the case of two particles, in the case of initial states  $|ini_3\rangle$  and  $|ini_4\rangle$  and for interactions strengths for which the density flow is suppressed, the eigenstate decomposition is characterized by  $\kappa \approx 2$  (figure 8(d)) and the two dominant states can be consequently well-expressed as superpositions of the initial states  $|ini_{3,4}\rangle$  and their mirror reflections  $|ini'_{3,4}\rangle$ , respectively. On the other hand, in the case of initial states with opposite-spin particles occupying the same site ( $|ini_5\rangle$  and  $|ini_6\rangle$ ) the eigenstate decomposition is essentially different (figure 8(e)) and shows a smooth increasing trend with the interactions. In consequence, the many-body dynamics cannot be reduced to the simplified two- or few-level system and is much richer.

## 6. Four-particle system

Finally, we discuss the dynamics of four-particle system with balanced ( $N_\uparrow = N_\downarrow = 2$ ) and imbalanced ( $|N_\uparrow - N_\downarrow| = 2$ ) two-component situations. Here, the dynamics will depend on several factors such as particle number imbalance, mass-imbalance and the type of initial states (paired and unpaired) under consideration. To make the discussion more systematic and clear we first discuss the dynamics for the particle

imbalance systems with unpaired initial states and then we analyze the balanced ( $N_\uparrow = N_\downarrow = 2$ ) system with the same kind of configuration. Next to the dynamics of the unpaired initial states, we discuss the paired situation for the balanced and imbalanced particle numbers cases.

The dynamical scenario of the particle imbalanced system can be thought as the dynamics of an impurity atom (lighter or heavier) in contact with a fermionic bath. The unpaired initial states are denoted as  $|\text{ini}_7\rangle = a_{L0}^\dagger a_{L1}^\dagger a_{L2}^\dagger b_{R0}^\dagger |\text{vac}\rangle$  and  $|\text{ini}_8\rangle = a_{R0}^\dagger b_{L0}^\dagger b_{L1}^\dagger b_{L2}^\dagger |\text{vac}\rangle$ . Schematic view of the initial states  $|\text{ini}_7\rangle$  is for instance shown in the figure 3(e). The many-body spectra for both type of particle-imbalanced systems and the behavior of the initial states  $|\text{ini}_7\rangle$  and  $|\text{ini}_8\rangle$  with respect to the interaction are qualitatively similar to the three particle case.

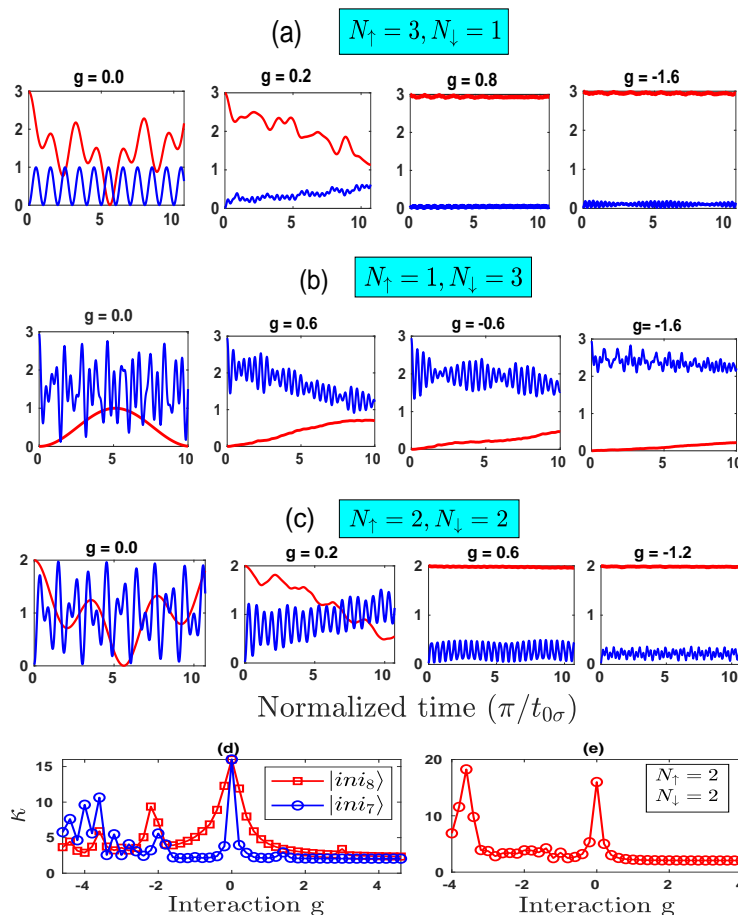


**Figure 9.** (Color online) Left-well occupation dynamics of the unpaired four particle systems with various initial states: (a)  $N_\uparrow = 3, N_\downarrow = 1$  and  $|\text{ini}_7\rangle$ , (b)  $N_\uparrow = 1, N_\downarrow = 3$  and  $|\text{ini}_8\rangle$ , (c)  $N_\uparrow = 2, N_\downarrow = 2$  with initial state shown in Fig. 3g. Blue and red curves are for the lighter and heavier component respectively. In the lower panel (d and e) we have compared the  $\kappa$  values as a function of interaction parameter for these initial states.

The time evolution of the left-well occupation number  $N_{L\sigma}(t)$  for the initial states

$|\text{ini}_7\rangle$  is presented in figure 9(a). Since it is natural to expect that as the number of particles for the state  $|\text{ini}_3\rangle$  is different than  $|\text{ini}_7\rangle$  so the dynamics can be affected notably due to particle number imbalance. However, we see the behavior of three and four-particle systems with more number of heavier components are very similar. For instance, the system shows dominant tunneling only for a smaller value of interactions ( $|g| \lesssim 0.4$ ) driven by the mutual effect of single-particle tunneling and the interaction terms of the Hamiltonian. From our exact diagonalization analysis we find for the state  $|\text{ini}_7\rangle$  the suppressed tunneling regions are realized for attraction lower than  $g \sim -2$  and for  $g > 0.4$  at the repulsive end. On the other hand, the finite tunneling region for the state  $|\text{ini}_8\rangle$  (see figure 9(b)) is little extended on both sides of the non-interacting limit before the tunneling is considerably suppressed. Our numerical results show for this state the dynamics is highly reduced for interactions beyond  $|g| \sim 0.8$ .

Unexpectedly, the dynamics of balanced four-particle system ( $N_\uparrow = 2, N_\downarrow = 2$ ) also shows analogous behavior to the unbalanced case of the spatially separated situation. For example, the dynamics shows maximum tunneling probability for a smaller value of interactions (e.g.  $g$  value between  $\sim -0.5$  and  $\sim 0.4$ ) as shown in figure 9(c). The strong suppression of particles flow beyond this regime can be understood by comparing the average energy of the initial state with the many-body spectra. In fact, for repulsion larger than  $g \sim 0.4$ , there are no enough eigenstates of the system with energies close to the initial state to contribute and cause efficient tunneling. Quite similar situation occurs for attractive interactions in the regime  $-1.2 < g < -0.4$ . For stronger attractions, however, the initial state energy is immersed in the plethora of many-body eigenstates having close energies. In consequence, the dynamics become unpredictable due to its huge sensitivity to the initial state and tuning of the interaction strength.

The dynamical behavior is also reflected in the eigenstate decomposition of these initial states as given in figure 9(d)-(e), which show at the attractive side  $N_\uparrow = 3, N_\downarrow = 1$  system is more resonant in compared to  $N_\uparrow = 1, N_\downarrow = 3$ . Further, it is important to notice from this plot that at the repulsive side there is now resonant point appear for these four-particle systems which were absent in the lower particle systems. This resonance can also be deducted from the energy spectrum. For the balanced case, although the decomposition shows a smooth trend at the attractive side, the value  $\kappa \sim 5$  indicates the significant role of more than two eigenstates on the dynamics. This indicates with finite attractions the dynamics of the balanced system cannot be explained in terms of two-level approximation.

In figure 10(a)-(b), we compare the single-particle correlation between the  $N_\uparrow = 1, N_\downarrow = 3$  and  $N_\uparrow = 3, N_\downarrow = 1$  systems. From these entropy plots, it is crucial to realize that the correlation of the single heavier impurity with the lighter fermionic sea is comparatively larger than the lighter impurity atom with the heavier components. In fact, correlations are always build in the system of  $N_\uparrow = 1, N_\downarrow = 3$  particles for the whole range of repulsions. This fact is also perceived in the three-

particles cases though the order of correlation is smaller compared to the four-particle systems. Additionally, the resonance regime as observed in the dynamics of occupation number at the repulsive side is also clearly visible in the entropy plots for both types of systems.

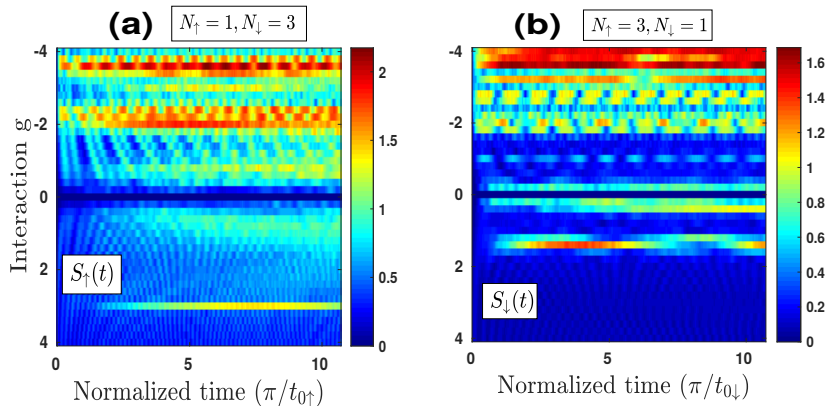


**Figure 10.** (Color online) (a) Dynamics of single-particle entropy for the heavier atom ( $S_{\uparrow}(t)$ ) in  $N_{\uparrow} = 1, N_{\downarrow} = 3$  system with initial state  $|\text{ini}_8\rangle$  and (b) for the lighter atom ( $S_{\downarrow}(t)$ ) in  $N_{\uparrow} = 3, N_{\downarrow} = 1$  system with  $|\text{ini}_7\rangle$ .

Let's now discuss the dynamical properties for the paired initial states of the particle imbalanced case, denoted by  $|\text{ini}_9\rangle = a_{L0}^{\dagger} a_{L1}^{\dagger} a_{R0}^{\dagger} b_{R0}^{\dagger} |\text{vac}\rangle$  and  $|\text{ini}_{10}\rangle = a_{R0}^{\dagger} b_{L0}^{\dagger} b_{L1}^{\dagger} b_{R0}^{\dagger} |\text{vac}\rangle$ . The schematic view of these initial states is shown in Figure 3(f). From the dynamics of the state  $|\text{ini}_9\rangle$  (see figure 11(a)) one can observe that in the non-interacting limit the particles oscillate with their natural frequencies. Due to the Pauli exclusion principle, the left-well occupation probability ( $P_L$ ) is always bounded  $1 \leq P_L \leq 2$  for the flavor with a larger number of particles. In other words, it is not feasible to excite the heavier atom from the ground band and induce tunneling with  $P_L > 2$ .

The dynamical behavior of this imbalanced and paired four particle system can effectively be thought as the two-particle system with a few leading order interaction terms. As for instance, in the state  $|\text{ini}_9\rangle$  the dynamics of the heavier and lighter components are primarily dependent on the leading order terms  $gU_{0000}$  and  $gU_{1001}$  involving the lowest and first excited mode of both wells. Note that the term  $gU_{0000}$  is always larger than the term  $gU_{1001}$  and for large  $g$  and therefore it is a leading interaction term. Moreover, for large enough  $g$  (around  $g \gtrsim t_{1\sigma}$ ) the term also dominates the single-particle tunneling terms. So, the effective interaction is approximately same for both the component. Therefore, intuitively the dynamics might be viewed as some coherent tunneling of both components in the large interaction limit. This intuition is indeed more evident from the figure 11 for relatively larger values of interaction strength,  $|g| \gtrsim 0.4$ . For low interaction value ( $|g| \lesssim 0.2$ ), the effect of single-particle tunnelings is dominant. Hence, the simultaneous effects of these terms lead to larger oscillation for lighter component and the dynamics will



be relatively different for both the flavors. We saw such low interaction behavior is completely resembled with the two-particle system in the initial state  $|\text{ini}_2\rangle$ . Thus, for larger interactions the dynamics mostly depend on interaction terms  $gU_{0000}$  and  $gU_{1001}$ , so the evolution can be understood as a combined dynamical process of initial states  $|\text{ini}_1\rangle$  and  $|\text{ini}_2\rangle$ . In a similar fashion, the time development of the system initially prepared in the state  $|\text{ini}_{10}\rangle$  can be understood using above arguments.

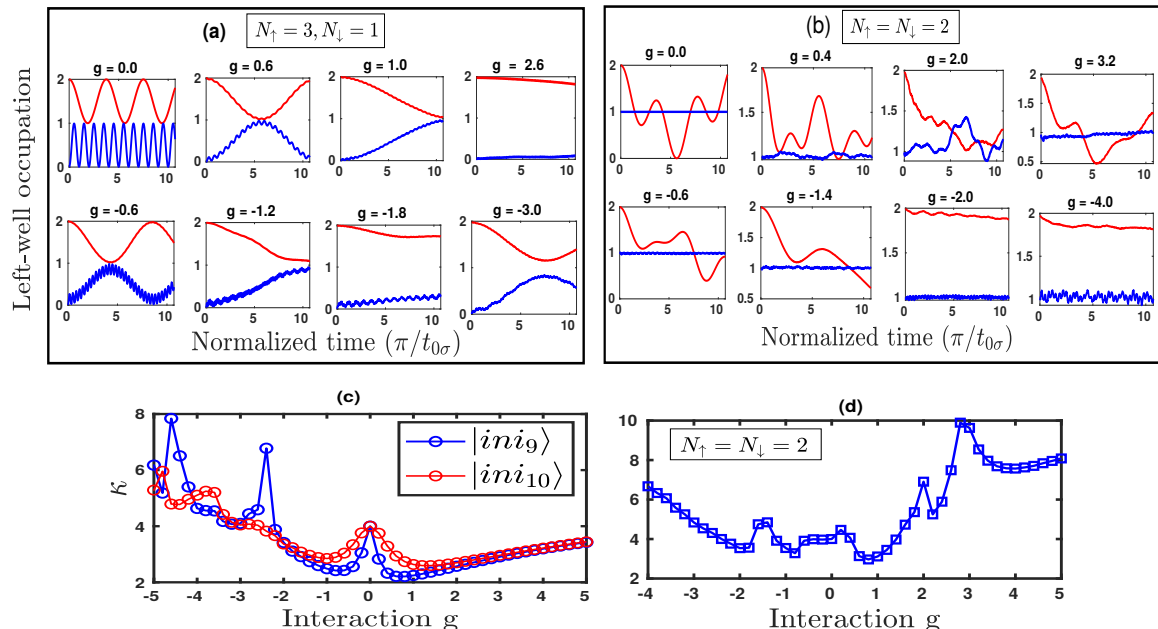


**Figure 11.** (Color online) Left-well occupation dynamics ( $N_{L\sigma}(t)$ ) for the imbalanced and balanced four particle systems in the paired situation: (a) the initial state  $|\text{ini}_9\rangle$  of  $N_\uparrow = 3, N_\downarrow = 1$  system (b)  $N_\uparrow = 2, N_\downarrow = 2$  system with initial configuration shown in figure 3(h). (c) and (d) are the eigenstate decomposition of these initial states as a function of interactions.

The dynamics for the balanced four-particle systems (see figure 11b) with paired configuration (see figure 3(h)) is quite different than the imbalanced counterpart. Here, the Pauli principle strongly restricts the tunneling of the lighter component to the lowest band for the whole range of attraction. The same principle also holds at the repulsive side, except some resonance points (the first is around  $g \sim 2.0$ ) where one can also find finite tunneling for the lighter atoms. On the other hand, there is always finite tunneling for the heavier flavor for any interactions.

The eigenstate decomposition of the paired initial states  $|\text{ini}_9\rangle$  and  $|\text{ini}_{10}\rangle$  is shown in figure 11(c). We see a smooth increase in the number of eigenstates that contribute to the initial state on both sides of the interaction, except for some resonance points in the attractive regime. As discussed above for the  $N_\uparrow = 3, N_\downarrow = 1$  system there is a negligible tunneling for the interaction in the range  $-2.0 < g < -1.4$  that correspond to  $2 < \kappa < 3$ . Also from the many-body spectra, we checked the average energy of the initial state is higher than any of these eigenstates. In fact,

there are no energy eigenstates close to the initial state energy. Similar arguments can be drawn to the repulsive part for  $g > 2.0$ . In this regime, although  $\kappa > 2$ , the lower eigenstates display two-fold degeneracies which effectively imply to  $\kappa = 2$ . Hence, the particles are highly localized in these eigenstates. At these values of interaction, violation of the energy conservation is more favored and consequently leads to the suppressed dynamics. For the balanced four-particle system, the decomposition (see figure 11(d)) shows resonance points on both sides of the non-interacting limit as discussed in the particle dynamics. For the whole range of repulsion,  $\kappa > 3$ , implies finite tunneling of the heavier component.

## 7. Dynamics of more than four particles system

The above mentioned dynamics for the system size up to four particles show a consistent results in the interaction regime  $-2.0 < g < 2.0$  within which the tunneling dynamics has a minimal dependency on very higher orbitals of the double-well. In fact, in our numerical approach we consider maximally 15 single-particle orbitals. Beyond this interaction regime the gradual dependency on the higher modes of the double-well is reflected in the dynamics. This dependency is more pronounced for the system with larger heavier components than the lighter one. As we have already realized, for the case of spatially separated initial configurations, the tunneling is dominated only for small enough interactions.

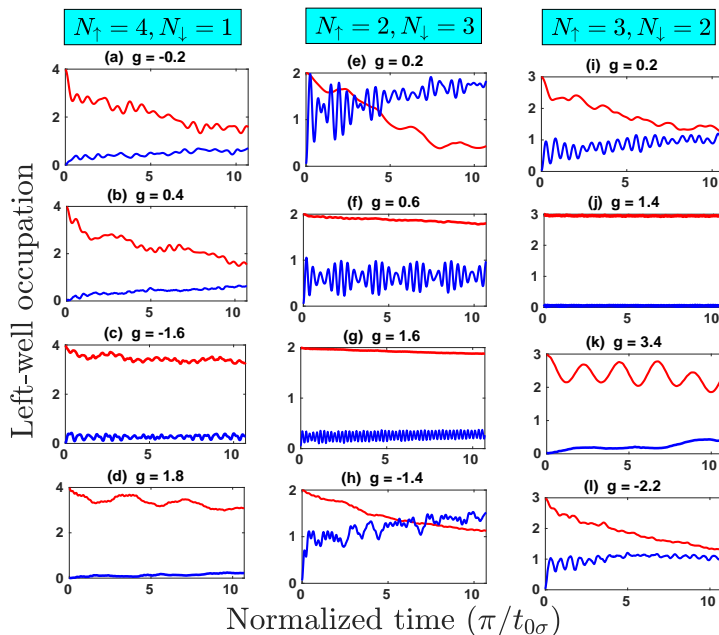


**Figure 12.** (Color online) Dynamics of five particle systems: Figures (a)-(d) refer to  $(N_{\uparrow} = 4, N_{\downarrow} = 1)$ , (e)-(h) correspond to  $(N_{\uparrow} = 2, N_{\downarrow} = 3)$  and (i)-(l) represent the  $(N_{\uparrow} = 3, N_{\downarrow} = 2)$  systems. The  $\mu$  values in all the systems are taken as  $40/6$ .

Therefore, it seems this low interaction behavior may be applicable to a reasonably larger system size where the two flavors are initially separated. To examine this fact, we also looked at some larger systems such as five-particle,  $N_\uparrow = 4, N_\downarrow = 1$ ;  $N_\uparrow = 3, N_\downarrow = 2$ ;  $N_\uparrow = 2, N_\downarrow = 3$  and six-particles  $N_\uparrow = 5, N_\downarrow = 1$  dynamics. The dynamics for some of them are given in figure 12. Besides this regime, for systems  $N_\uparrow = 3, N_\downarrow = 2$ ;  $N_\uparrow = 2, N_\downarrow = 3$  and  $N_\uparrow = 5, N_\downarrow = 1$  we also see finite tunneling for larger value of interactions as given in the figure 12(h), (k) and (l). As these interactions are well outside the above mentioned interaction regime, so for such values one can make consistent predictions only after including the effects from the higher orbitals which in fact computationally very demanding due to the exponentially growing Hilbert space size. Nevertheless, we expect such small interaction trend could be in general visible in few-body system with a reasonable number of particles.

## 8. Minimal basis models

For sufficiently small interactions, the physics of the above exact dynamics can also be understood by using a minimal basis sets for different system sizes. For example, the dynamics of the initial states  $|ini_1\rangle$  can be obtained simply using the two-mode approximation (*i.e.* taking into account only  $\psi_{L0}$  and  $\psi_{R0}$  orbitals). Hence, the minimal Fock basis for this case is  $B_1 \in \{a_{L0}^\dagger b_{R0}^\dagger, a_{R0}^\dagger b_{L0}^\dagger, a_{L0}^\dagger b_{L0}^\dagger, a_{R0}^\dagger b_{R0}^\dagger\}$  which leads to the simplified Hamiltonian

$$H^{B_1} = \begin{pmatrix} 0 & 0 & -t_{0\downarrow} & -t_{0\uparrow} \\ 0 & 0 & -t_{0\uparrow} & -t_{0\downarrow} \\ -t_{0\downarrow} & -t_{0\uparrow} & U_0^{LL} & 0 \\ -t_{0\uparrow} & -t_{0\downarrow} & 0 & U_0^{RR} \end{pmatrix} \quad (15)$$

where  $U_0^{LL}$  and  $U_0^{RR}$  are the interaction terms in the lowest orbitals of left and right wells. Similarly, one can write the reduced space Hamiltonian for the  $|ini_2\rangle$  by using the basis:  $B_2 \in \{a_{L1}^\dagger b_{R0}^\dagger, a_{R1}^\dagger b_{L0}^\dagger, a_{L1}^\dagger b_{L0}^\dagger, a_{R1}^\dagger b_{R0}^\dagger\}$ . The minimal models corresponding to the three- and four-particle cases, however, are obtained by taking into account the localized zeroth and first orbitals:  $\psi_{L0}, \psi_{L1}, \psi_{R0}$  and  $\psi_{R1}$ . The relevant truncated Fock basis for the initial state,  $|ini_3\rangle$ , will be then  $B_3 \in \{a_{L0}^\dagger a_{L1}^\dagger b_{R0}^\dagger, a_{R0}^\dagger a_{R1}^\dagger b_{L0}^\dagger, a_{L0}^\dagger a_{L1}^\dagger b_{L0}^\dagger, a_{R0}^\dagger a_{R1}^\dagger b_{R0}^\dagger, a_{L1}^\dagger a_{R0}^\dagger b_{R0}^\dagger, a_{L0}^\dagger a_{R1}^\dagger b_{L0}^\dagger, a_{L1}^\dagger a_{R0}^\dagger b_{L0}^\dagger, a_{L0}^\dagger a_{R1}^\dagger b_{R0}^\dagger\}$  for the  $N_\uparrow = 2, N_\downarrow = 1$  system. Analogously one can write down the reduced space for  $|ini_4\rangle$ . For a larger number of particles, one can follow the above procedure to construct the minimal basis for the initial states where the two flavors are spatially separated. So in general, the minimum number of orbitals that are needed to construct the minimal sets is equal to the number of orbitals up to the Fermi level and then one has to find out the basis vectors which leads to dominant interaction. However, in some cases, we even do not need all the basis vectors of the reduced Fock space. For example, this is the case when one needs to capture an appropriate description of the dynamics of the initial state  $|ini_6\rangle$ . The picture is somehow similar to

the  $|ini_2\rangle$  case where we just need four basis vectors and the only difference here is we have to incorporate some additional interaction terms.

## 9. Conclusion

We have thoroughly investigated the unitary dynamics of two-flavors fermions in the double-well potential with a maximum of the total number of particles up to six. Starting with a minimal system of just two particles we study the dynamics of other many-particle systems to understand the role of quantum statistics on dynamics. In particular, we have focused on the dynamical properties of two types of initially states which can also be easily prepared in the contemporary cold atoms experiments: the spatially separated two-components situation and in the second case one of the atoms from a chosen component is paired up with the other.

For the two-particle system, the dynamics is enhanced whenever the system's energy (the energy of the initial state) is close to eigenenergies of the many-body Hamiltonian. Then we observe acceleration in tunneling through the barrier. In contrast, the tunneling is almost completely suppressed far from these resonances. Beyond the two-particle system, in the presence of interactions, the dynamics is mostly suppressed for the spatially separated scenarios except for the particular interaction regime where the effect of single-particle tunneling is supported by the inter-component interactions. On the contrary, in the paired up situations, initial states energies are very sensitive to the interaction and hence, the dynamics is driven by the mutual interplay of interactions and single-particle tunnelings. The dynamical behavior of such a few fermionic systems is also analyzed through the many-body eigenstate decomposition of the initial state. Furthermore, by monitoring the evolution of the single-particle von Neumann entropy, we argue that independently on the suppression of the density flow quantum correlations are always built during the evolution.

## 10. Acknowledgments

This work was supported by the (Polish) National Science Center Grant No. 2016/22/E/ST2/00555. Numerical calculations were partially carried out in the Interdisciplinary Centre for Mathematical and Computational Modelling, University of Warsaw (ICM), under Computational Grant No. G75-6.

## 11. References

- [1] Thalhammer G, Winkler K, Lang F, Schmid S, Grimm R and Denschlag J H 2006 *Phys. Rev. Lett.* **96**(5) 050402 URL <https://link.aps.org/doi/10.1103/PhysRevLett.96.050402>
- [2] Köhl M, Moritz H, Stöferle T, Günter K and Esslinger T 2005 *Phys. Rev. Lett.* **94**(8) 080403 URL <https://link.aps.org/doi/10.1103/PhysRevLett.94.080403>

- [3] Serwane F, Zürn G, Lompe T, Ottenstein T B, Wenz A N and Jochim S 2011 *Science* **332** 336–338
- [4] Blume D 2012 *Reports on Progress in Physics* **75** 046401 URL <https://doi.org/10.1088/2F0034-4885/2F75/2F4/2F046401>
- [5] Wille E, Spiegelhalter F M, Kerner G, Naik D, Trenkwalder A, Hendl G, Schreck F, Grimm R, Tiecke T G, Walraven J T M, Kokkelmans S J J M F, Tiesinga E and Julienne P S 2008 *Phys. Rev. Lett.* **100**(5) 053201 URL <https://link.aps.org/doi/10.1103/PhysRevLett.100.053201>
- [6] Tiecke T G, Goosen M R, Ludewig A, Gensemer S D, Kraft S, Kokkelmans S J J M F and Walraven J T M 2010 *Phys. Rev. Lett.* **104**(5) 053202 URL <https://link.aps.org/doi/10.1103/PhysRevLett.104.053202>
- [7] Zinner, Nikolaj Thomas 2016 *EPJ Web of Conferences* **113** 01002 URL <https://doi.org/10.1051/epjconf/201611301002>
- [8] Sowiński T and García-March M Á 2019 *Reports on Progress in Physics* **82** 104401 URL <https://doi.org/10.1088/2F1361-6633/2Fab3a80>
- [9] Wenz A N, Zürn G, Murmann S, Brouzos I, Lompe T and Jochim S 2013 *Science* **342** 457–460 ISSN 0036-8075
- [10] Astrakharchik G E, Boronat J, Casulleras J and Giorgini S 2005 *Phys. Rev. Lett.* **95**(19) 190407 URL <https://link.aps.org/doi/10.1103/PhysRevLett.95.190407>
- [11] Sowiński T, Gajda M and Rzażewski K 2015 *EPL (Europhysics Letters)* **109** 26005 URL <https://doi.org/10.1209/2F0295-5075/2F109/2F26005>
- [12] D’Amico P and Rontani M 2015 *Phys. Rev. A* **91**(4) 043610 URL <https://link.aps.org/doi/10.1103/PhysRevA.91.043610>
- [13] Taglieber M, Voigt A C, Henkel F, Fray S, Hänsch T W and Dieckmann K 2006 *Phys. Rev. A* **73**(1) 011402 URL <https://link.aps.org/doi/10.1103/PhysRevA.73.011402>
- [14] Taglieber M, Voigt A C, Aoki T, Hänsch T W and Dieckmann K 2008 *Phys. Rev. Lett.* **100**(1) 010401 URL <https://link.aps.org/doi/10.1103/PhysRevLett.100.010401>
- [15] Erdmann J, Mistakidis S I and Schmelcher P 2018 *Phys. Rev. A* **98**(5) 053614 URL <https://link.aps.org/doi/10.1103/PhysRevA.98.053614>
- [16] Erdmann J, Mistakidis S I and Schmelcher P 2019 *Phys. Rev. A* **99**(1) 013605 URL <https://link.aps.org/doi/10.1103/PhysRevA.99.013605>
- [17] Efimov V N 1971 *Sov. J. Nucl. Phys.* **12** 589
- [18] Efimov V 1973 *Nuclear Physics A* **210** 157 – 188 ISSN 0375-9474 URL <http://www.sciencedirect.com/science/article/pii/0375947473905101>
- [19] Petrov D S, Salomon C and Shlyapnikov G V 2005 *Journal of Physics B: Atomic, Molecular and Optical Physics* **38** S645–S660 URL <https://doi.org/10.1088/2F0953-4075/2F38/2F9/2F014>
- [20] Kartavtsev O I and Malykh A V 2007 *Journal of Physics B: Atomic, Molecular and Optical Physics* **40** 1429–1441 URL <https://doi.org/10.1088/2F0953-4075/2F40/2F7/2F011>
- [21] Wu S T, Pao C H and Yip S K 2006 *Phys. Rev. B* **74**(22) 224504 URL <https://link.aps.org/doi/10.1103/PhysRevB.74.224504>
- [22] Iskin M and Sá de Melo C A R 2006 *Phys. Rev. Lett.* **97**(10) 100404 URL <https://link.aps.org/doi/10.1103/PhysRevLett.97.100404>
- [23] Lin G D, Yi W and Duan L M 2006 *Phys. Rev. A* **74**(3) 031604 URL <https://link.aps.org/doi/10.1103/PhysRevA.74.031604>
- [24] Orso G, Pitaevskii L P and Stringari S 2008 *Phys. Rev. A* **77**(3) 033611 URL <https://link.aps.org/doi/10.1103/PhysRevA.77.033611>
- [25] Parish M M, Marchetti F M, Lamacraft A and Simons B D 2007 *Phys. Rev. Lett.* **98**(16) 160402 URL <https://link.aps.org/doi/10.1103/PhysRevLett.98.160402>
- [26] Iskin M and Sá de Melo C A R 2008 *Phys. Rev. A* **77**(1) 013625 URL <https://link.aps.org/doi/10.1103/PhysRevA.77.013625>
- [27] Loft N J S, Dehkharghani A S, Mehta N P, Volosniev A G and Zinner N T 2015 *The European Physical Journal D* **69** 65 ISSN 1434-6079 URL <https://doi.org/10.1140/epjd/e2015-50845-9>
- [28] Pećak D, Gajda M and Sowiński T 2016 *New Journal of Physics* **18** 013030 URL

- <http://stacks.iop.org/1367-2630/18/i=1/a=013030>
- [29] Dehkharghani A S, Volosniev A G and Zinner N T 2016 *Journal of Physics B: Atomic, Molecular and Optical Physics* **49** 085301 URL <https://doi.org/10.1088%2F0953-4075%2F49%2F8%2F085301>
- [30] Pecak D and Sowinski T 2016 *Phys. Rev. A* **94**(4) 042118 URL <https://link.aps.org/doi/10.1103/PhysRevA.94.042118>
- [31] Sheehy D E and Radzihovsky L 2006 *Phys. Rev. Lett.* **96**(6) 060401 URL <https://link.aps.org/doi/10.1103/PhysRevLett.96.060401>
- [32] Zwierlein M W, Schunck C H, Schirotzek A and Ketterle W 2006 *Nature* **442**(6) 54 URL <https://doi.org/10.1038/nature04936>
- [33] Partridge G B, Li W, Kamar R I, Liao Y a and Hulet R G 2006 *Science* **311** 503–505 ISSN 0036-8075
- [34] Josephson B 1962 *Physics Letters* **1** 251 – 253 ISSN 0031-9163 URL <http://www.sciencedirect.com/science/article/pii/0031916362913690>
- [35] Shockley W 1949 *The Bell System Technical Journal* **28** 435–489
- [36] Esaki L 1958 *Phys. Rev.* **109**(2) 603–604 URL <https://link.aps.org/doi/10.1103/PhysRev.109.603>
- [37] Andrews M R, Townsend C G, Miesner H J, Durfee D S, Kurn D M and Ketterle W 1997 *Science* **275** 637–641 ISSN 0036-8075
- [38] Smerzi A, Fantoni S, Giovanazzi S and Shenoy S R 1997 *Phys. Rev. Lett.* **79**(25) 4950–4953 URL <https://link.aps.org/doi/10.1103/PhysRevLett.79.4950>
- [39] Milburn G J, Corney J, Wright E M and Walls D F 1997 *Phys. Rev. A* **55**(6) 4318–4324 URL <https://link.aps.org/doi/10.1103/PhysRevA.55.4318>
- [40] Menotti C, Anglin J R, Cirac J I and Zoller P 2001 *Phys. Rev. A* **63**(2) 023601 URL <https://link.aps.org/doi/10.1103/PhysRevA.63.023601>
- [41] Meier F and Zwerger W 2001 *Phys. Rev. A* **64**(3) 033610 URL <https://link.aps.org/doi/10.1103/PhysRevA.64.033610>
- [42] Shin Y, Saba M, Pasquini T A, Ketterle W, Pritchard D E and Leanhardt A E 2004 *Phys. Rev. Lett.* **92**(5) 050405 URL <https://link.aps.org/doi/10.1103/PhysRevLett.92.050405>
- [43] Albiez M, Gati R, Fölling J, Hunsmann S, Cristiani M and Oberthaler M K 2005 *Phys. Rev. Lett.* **95**(1) 010402 URL <https://link.aps.org/doi/10.1103/PhysRevLett.95.010402>
- [44] Burchianti A, Scazza F, Amico A, Valtolina G, Seman J A, Fort C, Zaccanti M, Inguscio M and Roati G 2018 *Phys. Rev. Lett.* **120**(2) 025302 URL <https://link.aps.org/doi/10.1103/PhysRevLett.120.025302>
- [45] Dobrzyniecki J and Sowiski T 2018 *Physics Letters A* **382** 394 – 399 ISSN 0375-9601 URL <http://www.sciencedirect.com/science/article/pii/S0375960117312070>
- [46] Bloch I 2005 *Nature Physics* **1** 23–30 ISSN 1745-2481 URL <https://doi.org/10.1038/nphys138>